Advanced Steel Construction – Vol. 20 No. 4 (2024) 376–384
DOI:10.18057/IJASC.2024.20.4.5

A BAYESIAN-OPTIMIZED NEURAL NETWORK MODEL FOR SHEAR CAPACITY OF A PERFOBOND STRIP CONNECTOR IN VARIOUS TYPES OF COMPOSITE STRUCTURES

Minh Hai Nguyen and Hoang Nam Phan *

Faculty of Road and Bridge Engineering, The University of Danang - University of Science and Technology, Da Nang, Viet Nam
** (Corresponding author: E-mail: phnam@dut.udn.vn)*

ABSTRACT

Perfobond strips are integral to composite steel-concrete structures or joints between precast concrete elements. However, the diverse boundary conditions and design parameters in various applications have led to numerous empirical and analytical methods to investigate their shear behavior. Existing empirical formulas often fail to accurately assess the shear capacity of perfobond strip connectors under different conditions. This study addresses this issue by developing a comprehensive prediction model for the shear capacity of perfobond strip connectors using a Bayesian-optimized artificial neural network (ANN). The proposed model evaluates shear capacity under various conditions, including the presence or absence of penetrating rebar in perforations, the use of normal or fiber-reinforced concrete, and various experimental specimen shapes applied in different composite structures. By utilizing an extensive dataset of 253 specimens, including 136 previously tested by the authors, the model is trained and optimized with a Bayesian optimization algorithm using a Gaussian process prior. This approach explores a wide range of hyperparameters to achieve optimal performance. The results show that the model excels in predicting the shear capacity of perfobond strip connectors across different design parameters and experimental conditions. A subsequent parametric study confirms the model's consistency with the shear-resisting mechanism of perfobond strips, underscoring the reliability and effectiveness of the ANN-based model. This model serves as a valuable tool for accurately predicting shear capacity in perfobond strip connectors across diverse design scenarios.

ARTICLE HISTORY

Received: 17 February 2024
Revised: 21 August 2024
Accepted: 5 September 2024

KEYWORDS

Perfobond strip;
Bayesian optimization;
Artificial neural network;
Shear capacity;
Sensitivity analysis;
A technical paper

1. Introduction

To ensure stress transfer between the steel and concrete components in composite structures, it is common to use shear connectors [1]. While headed studs have been the most used shear connectors [2, 3], the perfobond strip (called Perfobond Lestein in German, abbreviated as PBL) proposed by Leonhardt, et al. [4] has been increasingly utilized for various types of composite structures due to its unique advantages, such as high stiffness, good fatigue resistance [5], simple shape and flexible construction methods. Originally developed as a shear connector for composite girders, the PBL involves welding a steel plate with multiple perforations onto the top flange of the steel girder, as shown in Fig. 1(a). Concrete is then poured onto the concrete slab to fill the perforations, providing shear capacity that integrates the steel girder and concrete slab.

Since its development for the first application in composite girder bridge, many types of applications of the PBL have been developed. Among them, in the corrugated steel web of composite bridges, a PBL is used as shown in Fig. 1(b) [6-8]. In truss steel web composite bridges, PBL connectors are used at the joint between truss steel and concrete members, as shown in Fig. 1(c) [9]. Furthermore, in a composite deck designed to reduce the thickness of the bridge slabs and improve its fatigue durability, PBL connectors are also commonly used, as shown in Fig. 1(d) [10-12]. In these applications, the penetrating rebars are often placed in the perforations of the PBL to enhance the shear capacity and the stiffness of the shear connectors. In addition, Fig. 1(e) and Fig. 1(f) show examples of the PBL application in the rigid connection of the steel girder-concrete pier [13], and the steel-concrete hybrid pier [14], respectively. Furthermore, Fig. 1(g) shows an example of the application of the PBL to the joint of a prestressed concrete girder and steel girder in hybrid girder bridges with a proven application record in multi-span continuous girder bridges [15, 16]. Note that, in structures such as those shown in Fig. 1(e)-(g), the PBL is in concrete enclosed by a steel shell, so the PBL resists shear forces in the condition with the very highly confined condition.

With the advancements in manufacturing and construction technologies for precast concrete components in recent years, developing joints between these components has become increasingly important. One perspective-joining method that has gained prevalence in recent studies is the utilization of PBL connectors. These have been applied to joints between precast reinforced concrete slabs [17, 18], precast concrete barriers in bridges [19], and steel columns and precast concrete walls in buildings [20], as shown in Fig. 1(h) to Fig. 1(k). However, narrow joints are often preferred in these cases, making it difficult to arrange the surrounding reinforcement. To address this issue, PBLs are often used in conjunction with high-strength steel fiber concrete to ensure concrete workability in narrow spaces and prevent brittle joint failure in the absence of surrounding reinforcement [21].

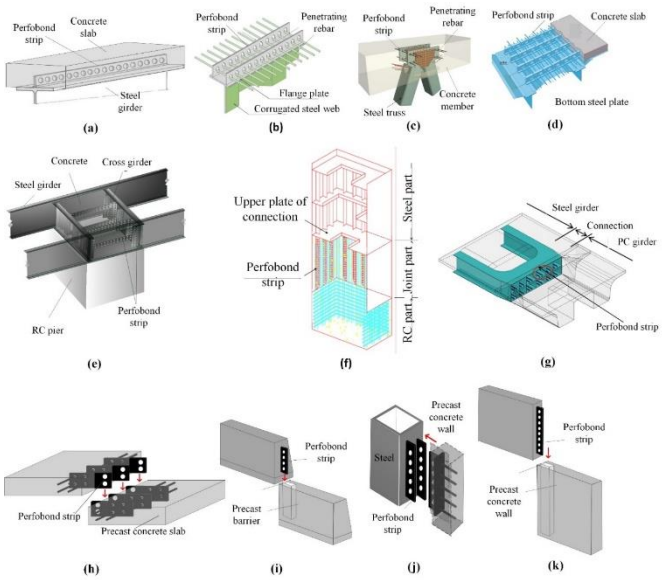

Fig. 1 Various applications of the PBLs: (a) Composite girder bridge; (b) Steel web PC bridge, (c) Steel truss web composite bridge; (d) Composite deck, (e) Rigid connection between pier and concrete slab, (f) Hybrid pier, (g) Hybrid girder bridge, (h) Joint of precast concrete slabs, (i) Joint of precast concrete barriers, (j) Joint between steel columns and precast concrete walls, and (k) Joint of precast concrete walls

As previously mentioned, PBL connectors have been utilized in a variety of applications, each with different usage conditions. Previous studies [22-28] have revealed that the shear capacity of PBL connectors is affected by several parameters, including the diameter and the number of perforations, the dimensions of perfobond steel plate, the diameter and the yield strength of penetrating rebar, the concrete strength, and particularly the confined conditions surrounding the PBL. In addition, the confined effect on the connector shear capacity depends on various factors, such as the specimen's concrete block dimension, specimen shape, support conditions during the loading test, and the arrangement of steel hoops or steel shells around the perfobond plate [29, 30]. Moreover, using high-strength fiber-reinforced concrete significantly increases confined effects in the absence of steel hoops [21]. However, most previous

studies offer empirical formulas to assess the shear capacity of PBL connectors based on a specific condition, without considering all the above parameters [4, 22, 23, 30-36]. As a result, these formulas only predict the shear capacity of PBL connectors in specific usage cases. Consequently, engineers may find it challenging to develop or design new and diverse uses of the PBL, as depicted in Fig. 1, using these formulas. Therefore, a more comprehensive prediction method is needed that accounts for the influence of a broader range of design parameters.

When a predicted value is influenced by multiple parameters, machine learning emerges as a promising method [37]. Recent studies have employed this technique to predict the shear capacity of PBL connectors. Allahyari, et al. [38] used an artificial neural network (ANN) to construct a prediction model based on the results of 90 collected test specimens. Sun, et al. [39] combined the backpropagation ANN model, the Genetic algorithm method, and the GSA method to develop a prediction model for the shear capacity of PBL connectors based on 107 specimens. However, most of the test specimens in these studies had a shape that corresponded to the use of the PBL in composite beams (Fig. 1(a)). This means that two perfobond steel plates were welded on both sides of the H-shaped steel, and the concrete slabs were symmetrically poured on both sides. As a result, these models fail to account for the shear capacity of PBL connectors in scenarios where the surrounding concrete experiences high confinement or when PBL is combined with high-strength fiber-reinforced concrete. This is because the parameters concerning the shape of the test specimens are not readily quantifiable, making it difficult to incorporate them into the machine learning models.

Therefore, this study aims to develop a comprehensive prediction model for the shear capacity of PBL connectors using an optimized neural network. While most previous studies have only proposed prediction models for the shear capacity under specific experimental conditions, including certain shapes and sizes of specimens, the novelty of this study lies in developing a model that can predict the shear capacity of PBL connectors under extensive experimental conditions, such as with or without penetrating rebar in the perforations, using normal or fiber-reinforced concrete, and especially for different shapes and dimensions of specimens. This allows engineers to use a single model to design the perfobond strip under various working conditions, thereby shortening the time needed to consider the correlation of each current design formula with the working conditions of the designed structure, requiring specialized knowledge to avoid errors when selecting inappropriate formulas.

Initially, a dataset comprising 253 specimens from various studies with diverse experimental conditions, including 136 from the authors' tests, was compiled, making it the largest dataset used in any study. This dataset was then utilized to systematize the shear-resisting mechanisms of perfobond strips, providing readers with a more comprehensive understanding of these mechanisms across different working conditions. Then, these results are also compared with the calculated values of eight existing empirical formulas to clarify the correlation between the calculated and experimental values as well as the limitations of each formula. To overcome the limitation of the existing models, an ANN model is then developed for the prediction of the shear capacity of PBL connectors, where a total of 12 input variables are considered in the training data. The model is also optimized based on a Gaussian process prior through a Bayesian optimization algorithm considering a large range of hyperparameters. Since the ANN model has been trained, a comprehensive parametric study is finally carried out, where the effectiveness of some primary parameters on the shear capacity of PBL connectors is evaluated and discussed in detail.

2. Collection of experimental data from the push-out and pull-out tests

Fig. 1 showcases the versatility of PBLs, widely employed in diverse applications. To investigate their shear capacity, researchers have proposed various test specimen shapes, as illustrated in Fig. 2. The five commonly used types, labeled A, B, C, D, and E, exhibit distinct configurations. While parameters like perforation diameter, number, steel plate dimensions, rebar diameter and yield strength, and concrete strength are variables across all specimens, there are also unique considerations for each type. Differences in the effects of confined surrounding concrete and the contribution of the bond between the steel plate and concrete contribute to varying shear capacities among the different PBL connector specimen types.

In A and D specimens, the concrete surrounding the PBL is located at the center. In contrast, in B and C specimens, the perfobond plate is welded onto a base steel plate and positioned at the edge of the concrete block. As a result, the confined effect of the surrounding concrete on the connector shear capacity is greater in A and D specimens than in B and C specimens, particularly when the concrete block is enclosed in a steel shell, as in D specimens [40]. Furthermore, the support conditions during the loading test differ across specimens. For A and D specimens, the reaction forces appear over the entire bottom surface of the concrete block, with the total vector of the reaction force coinciding with the loading direction. Conversely, the total reaction force vector of B, C, and E specimens is eccentric to the loading direction, inducing a moment on the concrete block that may affect the connector shear capacity in these cases [36]. Additionally, the interface between the steel plate and concrete is more extensive in B, C, and D specimens than in A and E specimens, leading to differences in the contribution of the bond between steel plates and concrete to the shear capacity of the PBL connector among these specimen types.

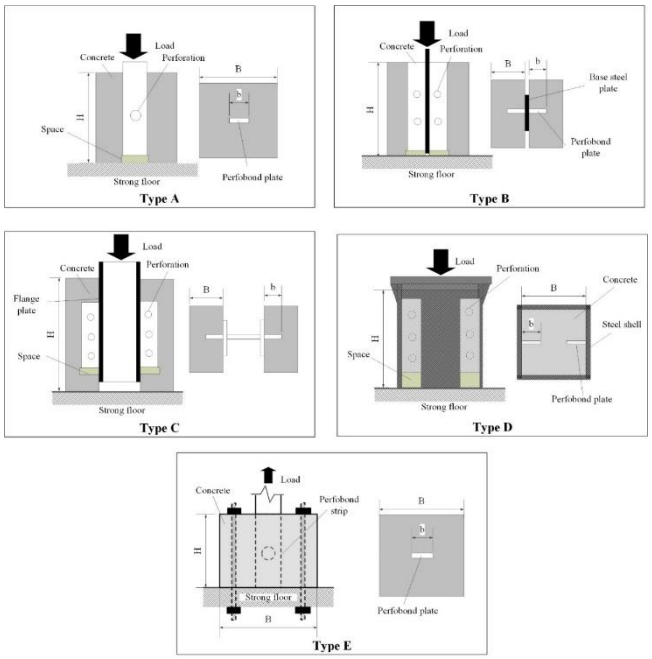

Fig. 2 Various types of test specimens for the PBL

Due to the variety of factors that affect the shear capacity of PBL connectors, most studies have only investigated its capacity within a certain range of usage. To construct a comprehensive prediction model that considers most of the necessary design parameters, this study collected and constructed a dataset of 253 experimental specimens, with a wide range of parameters as shown in Table 1 [21, 29, 32, 34-36, 41-53].

Among these specimens, 136 specimens were collected from the previous studies of the authors [21, 29, 34-36], with types A, B, and E, while the remaining specimens were collected from other studies. Twelve experimental parameters were considered, which is more than any previous model predicting the shear capacity of PBL connectors.

Table 1
Range of experimental parameters

No.	Parameters	Notation	Range
1	Specimen type	Shape	5 types (A – E)
2	Perfobond plate thickness	T (mm)	8-25
3	Perfobond plate width	a (mm)	60-300
4	Perfobond plate length	L (mm)	100-655
5	Number of perforations	n	1-5
6	Perforation diameter	D (mm)	30-90
7	Rebar diameter	d (mm)	0, 10-25
8	Concrete compressive strength	f_c (MPa)	14-105
9	Volumetric content of steel fibers in concrete	V_f (%)	0-2.3
10	Yield strength of penetrating rebar	f_y (MPa)	0, 329-410
11	Concrete block height	H (mm)	150-1000
12	Concrete block width	B (mm)	150-500

The dataset included 82 specimens that used penetrating rebars in the perforations and 172 specimens that did not. In addition, the dataset is composed of 5 different specimen shapes, with varying dimensions of the perfobond steel

plate, penetrating rebars, and concrete blocks. Notably, the compressive strength of the concrete ranged from 14-105 MPa, demonstrating that the dataset includes cases where the PBL is used in combination with high-strength concrete.

Fig. 3 displays the distribution of key parameters. It can be observed that the data is focused on the range of design parameters commonly used for the PBL. Specifically, the data for specimens with perforation diameters is uniformly distributed between 30-70mm, while only a few specimens have diameters larger than 70mm (Fig. 3(a)). This is because the PBL is typically used within the width limit of perfobond steel plates under 150mm, and the diameter of the perforation is usually limited to half the width of the perfobond steel plate. The diameter of the penetrating rebar is evenly distributed between 10-25mm in Fig. 3(b), while smaller diameter rebars are not used because they do not contribute much to the connector shear capacity.

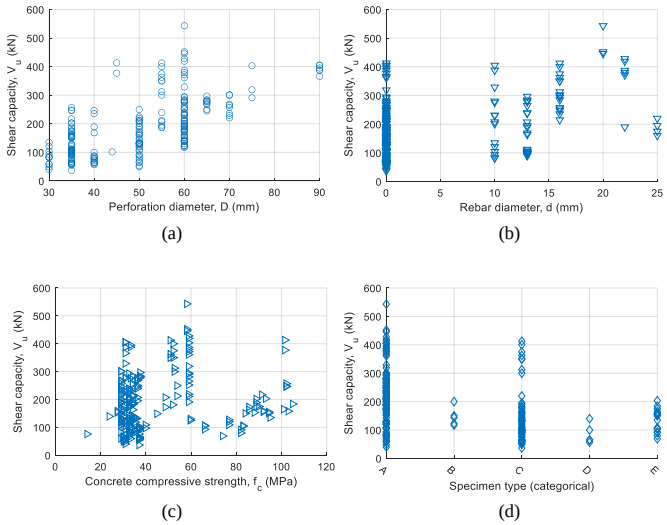

Fig. 3 Data distribution of main parameters related to shear capacity: (a) Perforation diameter, (b) Penetrating rebar diameter, (c) Concrete compressive strength, (d) Specimen types

Furthermore, the compressive strength data for concrete is mainly concentrated within the range of ordinary concrete, which is 25-60 MPa (Fig. 3(c)). However, there are also quite a few test specimens using high-strength concrete over 60MPa. On the other hand, the amount of data for specimen types A, C, and E is higher than that for types B and D. For type D specimens, the PBL is enclosed by a steel shell, which corresponds to a scenario where the concrete area around it has a very high confined condition, and this is rare in practical applications. Type B specimens are also rarely used because the stress transmission mechanism of this specimen is relatively similar to that of type C specimens. The effects of these parameters on the connector shear capacity, as well as the effect of the data distribution on the results of machine learning models, will be discussed in subsequent sections of the paper.

3. Shear resisting mechanism of the PBLs based on previous results

3.1. *Affecting mechanism of penetrating rebars*

Fig. 4(a), extracted from the authors' previous push-out tests [34, 35], presents examples of the relationship between shear force and slip for perfobond strips with a perforation diameter of 60 mm, both in cases without penetrating rebar (black lines) and with penetrating rebar of 13 mm diameter (red lines). It is noticed that other experimental parameters, such as concrete strength and the shape and size of the specimens, were kept consistent. The results indicate that the presence of penetrating rebar does not significantly influence the behavior in the initial stage of shear force, where the slip is below 3 mm; however, it does impact the subsequent stages of shear force. Based on this behavior, Fig. 4(b) idealizes the typical relationships between shear force and slip for both cases, with and without penetrating rebar.

For a case without penetrating rebar, the shear-resisting mechanism of the PBL can be divided into three stages: (1) the linear region, (2) the nonlinear region, and (3) the softening region. Fig. 4(c) visually presents stress components, revealing key observations:

In the linear region, PBL force is resisted by the bond at the steel plate-concrete interface and concrete shear force in the perforation. Initial stiffness is high but diminishes in stage (2) when the interface stress exceeds bond strength. Variations in specimen behavior arise from the steel plate-concrete interface, influencing both initial stiffness and the linear region's endpoint.

In the nonlinear region, PBL force is chiefly resisted by shear force on two concrete surfaces in the perforation. The maximum shear force, defining connector shear capacity, occurs upon shear fracture at these surfaces. Factors influencing capacity include perforation diameter, concrete strength, steel plate thickness, and confined conditions. The shape, size, support conditions, and the use of reinforcements or fiber-reinforced concrete also significantly impact shear capacity.

Post-shear fracture in stage (2), concrete confinement around the PBL prevents abrupt shear force decline. Greater confinement leads to a gradual decrease in shear force. This region's characteristics, often dependent on coarse aggregate dispersion in the perforation, are typically modeled as a straight line with a negative slope in shear force-slip models.

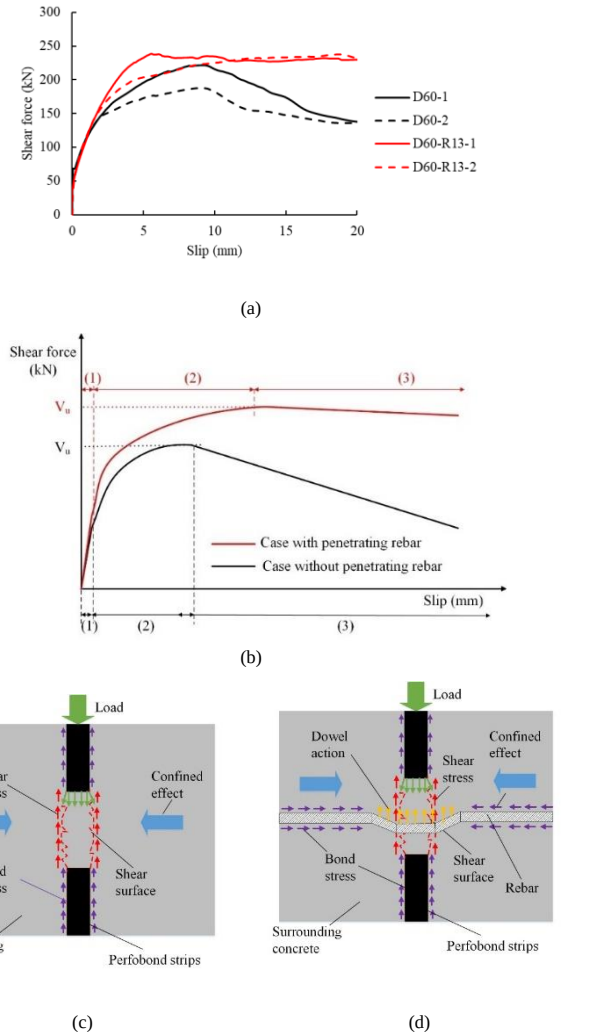

Fig. 4 Shear force–slip relationship of the PBLs: (a) Examples of the experimental shear force–slip relationships of the PBLs, (b) Model for shear force-slip relationship of the PBLs, (c) Shear resisting mechanism in the case without penetrating rebar, (d) Shear resisting mechanism in the case with penetrating rebar

In the presence of a penetrating rebar in the perforation, the mechanism remains similar during stage (1) as previously explained. However, the rebar significantly enhances shear capacity in stage (2) and prevents sudden shear force reduction after reaching capacity in stage (3). Fig. 4(c) illustrates the rebar's action, encompassing the dowel effect from rebar flexural deformation and the confined effect in the concrete around the PBL due to the rebar-concrete bond. The penetrating rebar's diameter notably impacts shear capacity, while the steel plate thickness influences stress distribution and, consequently, the rebar's flexural deformation range. Concrete strength also affects this deformation. The shear-resisting mechanism with penetrating rebar is more intricate than without, with parameters influencing shear capacity mutually. Despite this complexity, the rebar arrangement aids in averting brittle failure of the shear connector, making it prevalent in PBL applications with low confined concrete conditions and convenient rebar arrangement.

3.2. *Affecting mechanism of specimen types and block dimensions*

Most previous studies have conducted experiments using basic parameters,

such as concrete strength, perforation diameter, perfobond steel plate thickness, and the diameter of penetrating rebar, on specimens with fixed shapes and dimensions. However, even when these experimental parameters are identical, the shear capacity of the perfobond strip can still vary. To clarify this, Fig. 5(a) [34, 45, 46] illustrates the impact of specimen shape, corresponding to types A, B, and C in Fig. 2, while Fig. 5(b) [29] demonstrates the influence of the dimensions of the concrete block surrounding the perfobond strip in type A specimens. All test samples in these figures were derived from the authors' previous tests, with a perforation diameter of 60 mm, perfobond steel plate thickness of 12 mm, concrete compressive strength of approximately 30 MPa, and no penetrating rebar. It is evident that both the specimen shape and the concrete block dimensions significantly affect the shear capacity of the perfobond strip. This effect can be explained by the different confinement effects exerted by the concrete region surrounding the perfobond strip in the various test specimens, as shown in Fig. 5(c).

When shear force is transmitted to the concrete shear surface within the perforation, the uneven surface, caused by randomly distributed aggregates, generates a push-out force perpendicular to the perforation shear surface. This push-out force causes cracks to propagate into the surrounding concrete around the perfobond strip, ultimately reducing the shear capacity. In type A specimens, where the perfobond steel plate is centrally located within the concrete region, the confinement effect is generated from both sides of the strip, which is stronger than the effect generated from one side, as in type B and C specimens. This increased confinement effect restricts crack propagation into the surrounding concrete caused by the push-out force. Consequently, even with identical design parameters for the perfobond strip and concrete strength, the shear capacity of type A specimens remains higher than that of types B and C, as shown in Fig. 5(a).

Additionally, the confinement effect increases when the distance from the edge of the perfobond steel plate to the outer surface of the concrete block is larger. This explains why increasing the width of the concrete block significantly enhances the shear capacity of the perfobond strip, as demonstrated by the results in Fig. 5(b).

In summary, in addition to the basic design parameters, such as concrete strength, penetrating rebar, and perfobond strip dimensions, the boundary conditions and size of the concrete block surrounding the strip also significantly impact its shear capacity. This influence mechanism becomes more complex when multiple design parameters are varied simultaneously for different specimen types. Consequently, most current design formulas can assess the shear capacity of the perfobond strip under specific experimental conditions but show a low correlation with data when those conditions change, as will be discussed in Section 4 of this study.

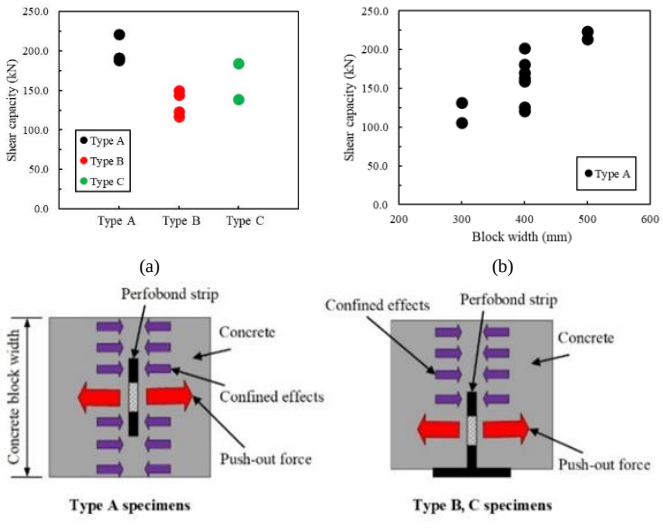

Fig. 5 Affecting mechanism of specimen types and block dimensions: (a) Effects of the specimen types on the shear capacity, (b) Effects of concrete block width on the shear capacity, (c) Schematics of the affecting mechanism

4. Evaluation of the existing shear capacity formulas of PBL connectors

4.1. Existing models for predicting the shear capacity of PBL connectors

Accurately predicting the shear capacity of PBL connectors is essential for designing shear connectors in composite steel-concrete structures and joints between precast concrete components. Consequently, multiple studies have focused on developing empirical formulas to predict the shear capacity of PBL connectors. Table 2 presents eight formulas proposed in previous studies [4, 22, 23, 30-36], arranged in chronological order of publication. Most of these formulas are based on statistical methods for experimental results, with experimental conditions and parameters varying within a specific range. Therefore, the range of applicability for each formula is determined based on the database used to construct it. However, to assess the applicability of these formulas over a broader range, the calculated values are compared with experimental results from a wide range of collected datasets, as described in a later section.

Table 2
Existing formulas for predicting the shear capacity of PBL connectors

1	Leonhardt, et al. [4]	For a case without penetrating rebar: $V_u = 2.553D^2 f_c$
2	Oguejiofor and Hosain [22]	$V_u = 4.5h_{sp}Tf_c + 0.91A_r f_y + 3.31D^2\sqrt{f_c}$
3	Ahn, et al. [23]	$V_u = 3.14h_{sp}Tf_c + 1.21A_r f_y + 1.895\pi D^2\sqrt{f_c}$
4	Chen [30]	$V_u = 1.38(D^2 - d_r^2)f_c + 1.24d_r^2 f_y$
5	JSCE [31]	For a case without penetrating rebar: $V_u = 1.6D^2 f_c$ For a case with penetrating rebar: $V_u = 1.85A - 26.1 \times 10^3$ In which, $A = \frac{\pi(D^2 - d_r^2)}{4}f_c + \frac{\pi d_r^2}{4}f_t$
6	He, et al. [32]	$V_u = \tau_b A_b + 1.06A_c f_c + 2.09A_r f_y$ In which, $\tau_b = -0.022f_c + 0.306\sqrt{f_c} - 0.573$
7	Zheng, et al. [33]	$V_u = 1.76(A - A_r)f_c + 1.58A_r f_y$
8	Nakajima and Nguyen [34-36]	For a case without penetrating rebar and using normal concrete: $V_u = 0.15\kappa_1 A f_c^{0.65} A_{sb}^{0.43} T^{-0.5}$ For the case without penetrating rebar and using high-strength steel fiber concrete: $V_u = \kappa_1\kappa_2\kappa_3 A f_c^{0.65}$ In which, κ_1 = 1.0 or 0.78, $\kappa_2 = 22V_f + 0.48$, $\kappa_3 = 0.22V_b^{0.24}$ for push-out force, and $\kappa_3 = 0.17V_b^{0.24}$ for pull-out force For a case with penetrating rebar and using normal concrete: $V_u = V_c + V_r$ In which, $V_c = 0.15\eta\kappa_1(A - A_r)f_c^{0.65}A_{sb}^{0.43}T^{-0.5}$ $V_r = 0.84d_r f_y D^{0.1}T^{0.8}$ $\eta = 6.9d_r^{0.4}D^{-0.7}$

Notes: V_u: Shear capacity per one perforation (N); D: Perforation diameter (mm); f_c: Concrete compressive strength (MPa); h_{sp}: Width of perfobond steel plate (mm); T: Thickness of perfobond steel plate (mm); A_r: Cross section of penetrating rebar (mm^2); f_y: Yield strength of penetrating rebar (MPa); d_r: Penetrating rebar diameter (mm); τ_b: Bond strength between steel plate and concrete (MPa); A_b: Steel plate-concrete interface area (mm^2); A_c: Area of concrete part in perforation (mm^2); A_{sb}: Side area of the concrete block surrounding the PBL (mm^2); κ_1: Influence coefficient of the test specimen's shape; κ_2: Influence coefficient of the volume content inside the concrete mixture; κ_3: Influence coefficient of the concrete block size; η: Interaction coefficient between concrete and penetrating rebar

Table 2 reveals that the coefficients in the formulas vary, but most formulas share a relatively similar form. The formula of Leonhardt, et al. [4], which introduced the PBL concept, has the simplest form as it only considers the effects of concrete strength and perforation diameter. This is because Leonhardt et al. initially developed the PBL concept for composite beams and penetrating rebar was not arranged in the perforation. Their formula is based on the results of the type C specimen test. However, due to its simplicity and ease of use for engineers, the committee on hybrid structures of the Japan Society of Civil Engineers [31] has adjusted the coefficients based on this form and incorporated them into the corresponding standard to predict the shear capacity of PBL connectors without penetrating rebar.

Oguejiofor and Hosain [22] proposed a method of using PBLs with penetrating rebar and intermittently welded perfobond steel plates on the steel girder flange, leading to three components that contribute to the connector shear capacity. These components include the bearing force at the perfobond steel plate's edge, the axial action of the penetrating rebar, and the concrete's shear force in the perforation. The contribution of each component is indicated by corresponding coefficients. Ahn, et al. [23] also developed a formula based on this concept but with coefficients adjusted based on expanded experimental data. It should be noted that the bearing force at the PBL edge is not considered in the calculation of the connector shear capacity for the specimens collected in this study. This is because a gap is established under the perfobond steel plate in all test specimens. Chen [30], He, et al. [32], and Zheng, et al. [33] also have similar forms but do not account for the end-bearing force at the perfobond plate's edge. Among them, the formula developed by He, et al. [32] considers the bond stress between the perfobond steel plate and concrete. Nakajima and Nguyen's formulas [34-36] have a basic structure that includes the concrete shear force in the perforation and the penetrating rebar's contribution. However, each component is more complex and considers more parameters than the other formulas, which are formulated based on an exponential function to assess the mutual influences of the parameters.

4.2. Statistical analysis of the correlation between empirical formulas and experimental data

Figs. 6(a)-(h) depict the correlation between the experimental shear capacity (target value) and the calculated values (output value) for each of the eight formulas presented in Table 2. The regression line is represented by the blue line in each figure, while the line $y = x$ is indicated by the black dotted line, signifying the point at which the calculated value equals the experimental value. The vertical axis of each figure displays the formula of the regression line. Fig. 7 presents the statistical analysis results for the data in Fig. 6, with the Min, Max, and Mean ratios indicated by the minus sign for each formula. The standard deviation of the data is represented by the height of the blue rectangle, while the red plus sign denotes whiskers, signifying the data points that fall outside the trend determined by the regression analysis.

Figs. 6(a)-(c) and Fig. 7 demonstrate that the formula of Leonhardt, et al. [4] overestimates the experimental shear capacity, whereas the formulas of Oguejiofor and Hosain [22] and Ahn, et al. [23] tend to underestimate the experimental values. The formula of Leonhardt, et al. [4] considers only the effects of perforation diameter and concrete strength and is based on a limited experimental dataset, which explains the discrepancy with the results of a more extensive dataset. In contrast, the formulas of Oguejiofor and Hosain [22], as well as Ahn, et al. [23], were developed based on specimens that include the end bearing force at the perfobond steel plate's edge. However, the calculated values in Figs. 6(b) and 6(c) do not account for this contribution since the test specimens used in this study have a gap established under the perfobond steel plate. Consequently, the resisting mechanism of the specimens in the database used to formulate the formulas of Oguejiofor and Hosain [22], as well as Ahn, et al. [23], differs from that of the specimens collected in this study, leading to a significant difference between the calculated and experimental values.

Fig. 7 indicates that the remaining formulas have average values in the range of 0.75 to 1.1, while Figs. 6(d) to 6(h) reveal that the correlation coefficients differ among the formulas. The formula proposed by Chen [30] exhibits the lowest average ratio due to the limited dataset used to develop their formula. Conversely, the formula proposed by JSCE demonstrates a high average ratio and the most skewed data, as it only considers the basic parameters and reference structure of the Leonhardt et al. formula, leading to a low correlation with the large experimental dataset that accounts for many complex influencing factors. The average values corresponding to the recently proposed formulas by He, et al. [32], Zheng, et al. [33], and Nakajima and Nguyen range from 0.8 to 1.0, as they are based on larger experimental datasets than previous formulas. However, the standard deviation of the data using He et al.'s formula is relatively high because of the bond strength between the steel plate and concrete, which has a large experimental error.

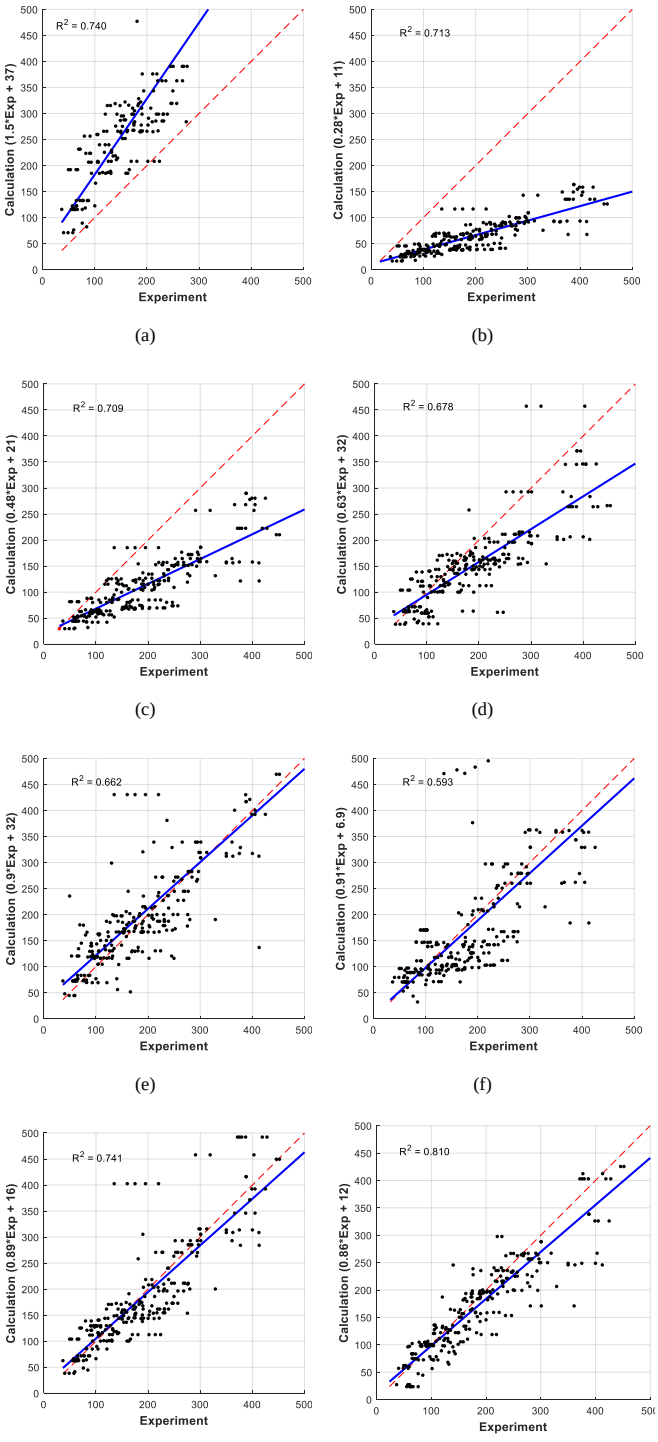

Fig. 6 Statistical analysis of the shear capacity ratio from existing formulas and experimental data: (a) Leonhardt et al., (b) Oguejiofor and Hosain, (c) Ahn et al., (d) Chen, (e) JSCE, (f) He et al., (g) Zheng et al., and (h) Nakajima and Nguyen.

On the other hand, Nakajima and Nguyen's formula indicates the best correlation with the experimental data based on all statistical parameters, such as the average value, correlation coefficient, standard deviation, and the number of skewed specimens, as it is based on a large database, considers many influencing factors by analyzing the PBL connector mechanism, and is suitable for the parameters of the connector within the common range. Nevertheless, the correlation coefficient in Fig. 6(h) is only 0.900, and there are still many skewed data points, especially those in the experimental shear capacity range above 300 kN and below 80 kN. This may be attributed to the fact that Nakajima and Nguyen's formula focuses only on the parameters of the connector within the common range, without considering cases where the perforation is too small or too large.

In conclusion, the correlation of most current experimental formulas with the experimental dataset is not high, primarily due to (i) the limited dataset used in the statistical analysis to develop the formulas and (ii) the difficulty in

considering all the influencing factors based on conventional statistical methods. Hence, machine learning may provide a feasible solution when the influencing factors are complex, and the experimental dataset is large enough.

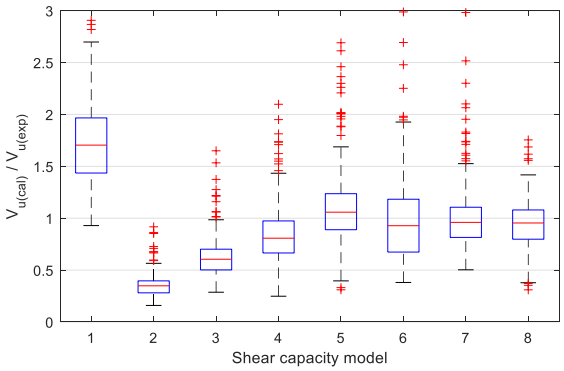

Fig. 7 Descriptive statistics of the ratio between the existing models and experimental data

5. Optimization of neural network model

5.1. ANN training data and feature selection

In the literature, various machine-learning models have been employed to tackle regression problems [40]. In this study, an ANN model is utilized for prediction purposes. The ANN architecture, as illustrated in Fig. 8, includes an input layer, one or more hidden layers, and an output layer, with fully connected neurons. The input layer is comprised of n neurons, which correspond to the input variables of the training data. The hidden layers can contain one or multiple layers, and each layer consists of several neurons. The selection of the number of hidden layers and neurons per layer is based on the complexity of the problem and performance evaluation. The output layer is made up of one or more neurons, with each neuron representing a predicted output. During the training process, the ANN adjusts the weights of the connections between neurons to minimize the difference between the predicted outputs and actual outputs of the training data.

The ANN model excels in capturing complex and nonlinear relationships between input variables and outputs. Prediction accuracy depends on the quality and quantity of training data, as well as model parameter selection. A well-trained and optimized ANN model can offer precise and robust predictions for regression problems.

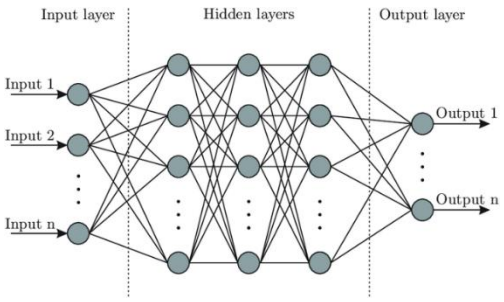

Fig. 8 Example of ANN architecture

This study uses 253 test results as training data, with 12 input variables and connector shear capacity as the output. Table 1 details the parameters and their ranges, with only specimen type labeled; other parameters are numeric. The data is split into a training set (85% or 215 data) and a test set (15% or 38 data). While the parameters in Table 1 are more comprehensive than in prior studies, some are not included. The yield or tensile strength of the steel plate is omitted, as failures primarily involve concrete shear or rebar fracture. Additionally, the reinforcement arrangement in the concrete block, a crucial parameter, varies widely in applications, complicating data collection. Furthermore, prior research by the authors has shown that this factor primarily contributes to preventing brittle failure rather than directly enhancing shear resistance [29, 34]. Hence, this parameter has been omitted. The influence of frictional force between the perfobond steel plate and concrete can be represented by parameters such as perfobond plate width and length. However, since the effect of frictional force between the base steel plate and concrete only appears in type B, C, and D specimens, and not in type A and E specimens, thereby it is not included. For type D specimens, this effect can be indirectly considered through the width and height of the concrete block. For type B and C specimens, as the width of the base plate varies minimally among specimens with the same type, the differences in the frictional force between the base steel plate and concrete among the specimens can also be indirectly assessed through the height of the concrete block. Therefore, the parameters related to the dimensions of the base steel plate are not listed.

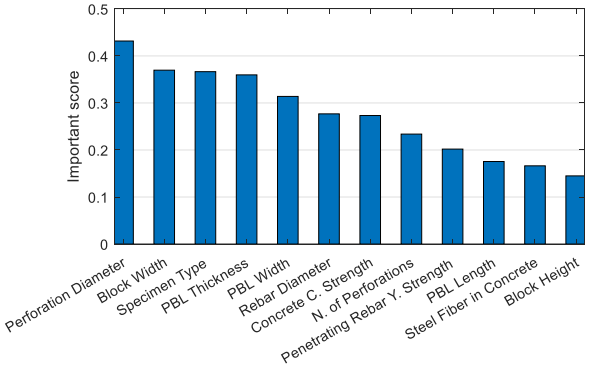

Fig. 9 Feature important scores sorted by the MRMR algorithm

The feature selection is first performed to identify the important score of each input feature on the response variable. The MRMR algorithm is used [54]. This algorithm seeks to identify an optimal feature set that is both maximally dissimilar and mutually exclusive, and that can effectively represent the response variable. The primary objective of the MRMR algorithm is to identify an optimal feature set S that maximizes the relevance of S to the response variable y while minimizing the redundancy of S. These two objectives are quantified using mutual information I. The optimal set S can be obtained by considering all $2^{|\Omega|}$ possible feature combinations, where Ω is the entire set of available features. However, the MRMR algorithm uses a forward addition scheme to rank features, which reduces the computation cost to $O(|\Omega| \cdot |S|)$ by utilizing mutual information quotient (MIQ) values,

$$MIQ_x = \frac{I(x,y)}{\frac{1}{|S|}\sum_{z \in S} I(x,z)}, \quad (1)$$

where the numerator and denominator are the relevance and redundancy of a feature, respectively, and $|S|$ is the number of features in S.

The function can be used to rank all features in Ω. The computation cost for this function is $O(|\Omega|2)$, and it uses a heuristic algorithm to quantify the importance of each feature, returning a score that indicates the significance of each predictor.

MRMR analysis findings in Fig. 9 reveal the influence of 12 input parameters on connector shear capacity. Beyond parameters like perforation diameter and concrete strength, those linked to the confined condition around the PBL (e.g., block width or specimen type) significantly affect shear capacity. Neglecting this can lead to deviations in calculated values. Dimensions of the perfobond steel plate, like thickness and width, exert substantial influence due to the bond with concrete. Steel plate thickness impacts stress distribution and shear surface formation, influencing capacity. Parameters related to specimen height have a lower impact, suggesting that multiple perforations on the steel plate minimally affect shear capacity per perforation.

5.2. Optimizable neural network

During the process of training a machine learning model or neural network, a crucial step is selecting values for parameters such as learning rate, epochs, number of layers, and hidden units. The selection of reasonable parameters often relies on experience, and for each set of parameters, we must train the model, observe the results achieved, evaluate the results, adjust the parameters, and repeat the process. To automate this process, search algorithms such as Grid Search or Random Search are used [55]. However, these algorithms are only effective with a small number of parameters because the search space increases rapidly with many parameters, making the search time-consuming. Bayesian optimization is an algorithm that optimizes effectively for objective functions with large evaluation costs (such as training a neural network) based on the Bayesian theorem [56]. Bayesian optimization significantly reduces the number of trials compared to Grid Search or Random Search [56]. The following is an algorithm for Bayesian optimization with a Gaussian process prior:

Define the objective function $f(x)$ and specify the prior distribution over the objective function. This is typically done by assuming a Gaussian process prior over $f(x)$.

Define an acquisition function $\alpha(x)$ that measures the utility of sampling x. Popular acquisition functions include upper confidence bound, expected improvement, and probability of improvement.

For $t = 1, 2, \ldots, t_{max}$ (t_{max} is the maximum number of iterations):

Fit a Gaussian process model to the available data (x, y), where $y = f(x) + noise$. The model provides a posterior distribution over $f(x)$ given the observed data.

Select the next point to sample by maximizing the acquisition function: $x_t = argmax\, \alpha(x|D_{t-1})$, where D_{t-1} is the data up to time $t-1$.

Sample the objective function at x_t: $y_t = f(x_t) + noise$.

Add the new data point (x_t, y_t) to the observed data.

Finally, return the best-observed value of $f(x)$.

Table 3
Optimization analysis result

Hyperparameter	Value
Number of hidden layers	2
Activation function	Relu
Layer biases initializer	Ones
Layer weights initializer	He
Regularization strength	2.549
Number of neurons per hidden layers 1-2	210, 58

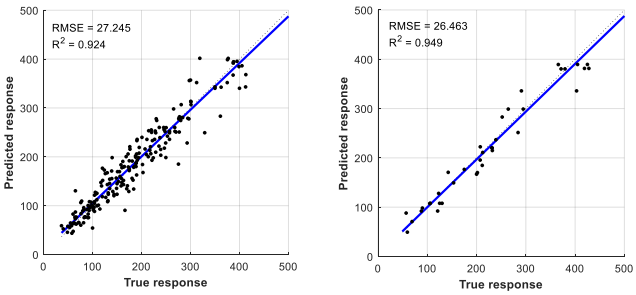

(a) (b)

Fig. 10 Regression plot of the calculated and actual values

To optimize the ANN model, a range of hyperparameters needs to be defined. In this study, the range of hyperparameters for the ANN model is introduced including the number of hidden layers (1, 2, and 3), the first, second-, and third-layer size (1-253 neurons), the activation function (ReLU, Tanh, Sigmoid), the layer biases initializer (Zeros, Ones), layer weights initializer (Glorot, He) [57, 58] and the regulation strength $(1e^{-5}/n, 1e^{5}/n)$, n is the number of observations. The iteration limit is fixed to 1000, and the train neural network regression model is adopted; this model is used to train a feedforward, fully connected neural network. The number of iterations of the Bayesian optimization is set as 100, and the acquisition function is selected as the expected improvement. For the validation, 5-fold cross-validation is used [59]. The result of the Bayesian optimization as the optimal hyperparameter for the ANN model is shown in Table 3, which comprises an optimal ANN model for the prediction.

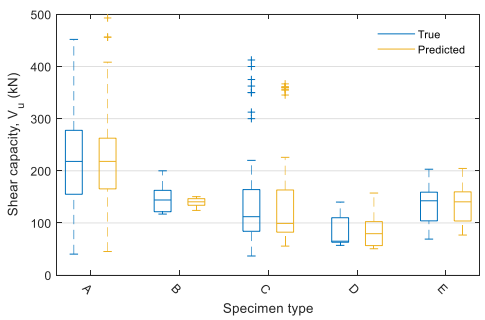

Fig. 11 Descriptive statistics of true and predicted values for specimen types

In addition to the validation using the 5-fold cross-validation on the training set, a separate test set of 15% data is used to test the model performance. The regression plots of the predicted and actual values from the 5-fold cross-validation and the test set are shown in Fig. 10 and an example of descriptive statistics of true and predicted values for specimen types is shown in Fig. 11. As observed from the figures, R^2 values are 0.924 and 0.948 for both the cross-validation and the separate test set, respectively, remarkably higher than that of the existing models previously mentioned. This demonstrates the high performance of the ANN model in predicting the shear capacity of PBL connectors in steel-concrete composite structures.

6. Effectiveness of primarily design parameters on shear capacity

The influence of key parameters on connector shear capacity was investigated using the developed model in Section 4. Figs. 12(a) to 12(e) present the impact of perforation diameter, penetrating rebar diameter, concrete compressive strength, perfobond plate thickness, and concrete block width. Type D specimens were excluded due to their limited quantity.

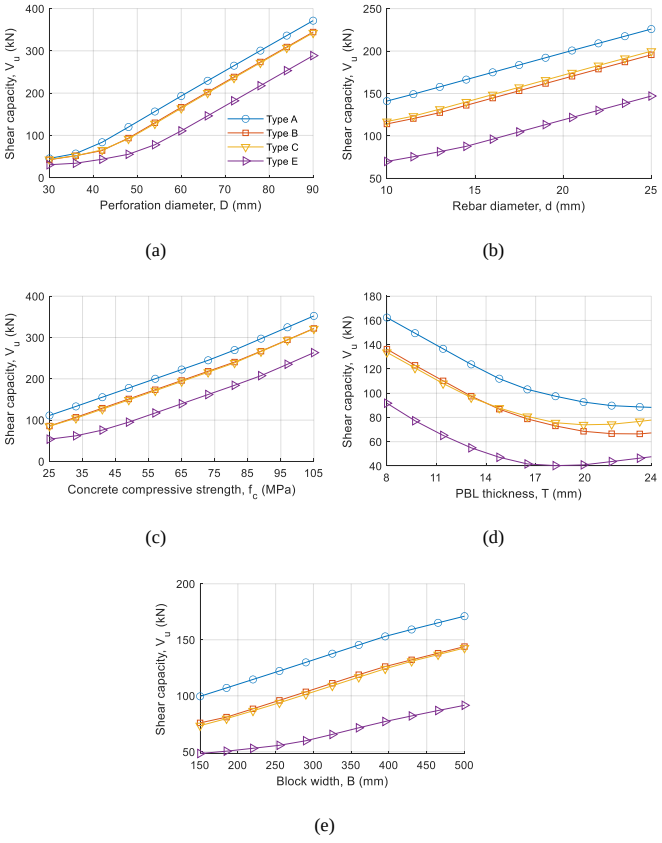

(a) (b) (c) (d) (e)

Fig. 12 ANN model-based parametric study results in terms of (a) Perforation diameter (b) Rebar diameter, (c) Concrete compressive strength, (d) PBL thickness, and (e) Block width

Results in Fig. 12 show that, with identical design parameters, type A has the highest shear capacity, followed by types B and C, with type E having the lowest. This aligns with load-bearing mechanisms discussed in Sections 2 and 3.1, emphasizing the importance of selecting an appropriate specimen type matching real conditions for accurate shear capacity calculations in design.

Observations in Fig. 12(a) indicate a non-linear increase in shear capacity with perforation diameter, suggesting expression in terms of the perforation area or square of the diameter, common in empirical formulas (Table 2). Conversely, the relationship between shear capacity and penetrating rebar diameter is nearly linear across all specimen types. Thus, it's recommended to express this relationship in terms of the diameter, reflecting the dowel action's dependence on rebar flexural deformation and diameter, as demonstrated in Nakajima and Nguyen's proposed formula.

Fig. 12(c) shows a nearly linear relationship between shear capacity and concrete compressive strength, consistent across normal-strength and high-strength concrete. Empirical formulas in Table 2 use various approaches to represent this effect, such as square root or exponential functions. However, the combined influence of concrete compressive strength on shear strength in the perforation and the confined effect on surrounding concrete is evaluated through its actual value.

Equations (1) to (7) in Table 2 overlook the impact of perfobond steel plate thickness on the shear force in the perforation and the contribution of the penetrating rebar. Conversely, Nakajima and Nguyen's formula highlights that increasing steel plate thickness reduces shear force but enhances the dowel effect. The observed trend in Fig. 12(d) aligns with Nakajima and Nguyen's study and emphasizes the importance of steel plate thickness.

Concrete block width consistently influences confined effects around the PBL, enhancing shear stress on two shear surfaces. This effect is neglected in Equations (1) to (7) but considered in Equation (8), making Nakajima and Nguyen's formula more correlated with the experimental data.

In summary, the parametric study aligns with the shear-resisting mechanism explained in Sections 2 and 3.1, confirming the reliability of the proposed machine learning-based model for a large experimental dataset, both statistically and in terms of the PBL's shear-resisting mechanism.

7. Conclusions

This study aims to develop a comprehensive prediction model for the shear capacity of PBL connectors using an optimized neural network. The research conducted a thorough investigation and meticulous data collection to create a dataset of 253 specimens from various sources, including 136 contributed by the authors, which is more than any other previous study. Based on this extensive dataset, the research systematically examined the shear-resisting mechanism of the perfobond strip and critically analyzed eight existing empirical formulas. This helps engineers gain a more comprehensive and deeper understanding of the shear resistance mechanism of the perfobond strip, as well as the strengths and limitations of the existing design formulas. The comparative analysis revealed inherent limitations in existing formulas, attributing their diminished correlation with experimental values to the challenges posed by a limited dataset and the complexity of incorporating all influencing factors through conventional statistical methods.

While most previous studies have only proposed prediction models for the shear capacity under specific experimental conditions, including certain shapes and sizes of the specimens, the novelty of this study lies in developing a model that can predict the shear capacity of PBL connectors under more comprehensive working conditions, such as with or without penetrating rebar in the perforations, using normal or fiber-reinforced concrete, and especially for different shapes and dimensions of test specimens. To achieve this objective, a feature selection analysis identified 12 input parameters and found that perforation diameter, block width, specimen type, and PBL thickness are significant contributors to the shear capacity of PBL connectors. Employing the Bayesian optimization algorithm, an optimized ANN model with a two-layer architecture demonstrated exceptional predictive performance, attaining an impressive R^2 value of 0.949 on a separate test set. This result demonstrates superiority over most existing prediction models, especially since this model can also predict the shear capacity of the perfobond strip with a more comprehensive range of applications.

The parametric study results consistently aligned with the shear-resisting mechanism of PBL, reinforcing the credibility and applicability of the proposed machine learning-based model across a broad experimental dataset. In light of these findings, this study not only advances the understanding of PBL connector behavior but also contributes a comprehensive prediction model with practical implications. This model stands poised for integration into engineering practices, offering a valuable tool for optimizing the design and analysis of concrete structures.

References

[1] X. Zeng, S.-F. Jiang, and D. Zhou, "Effect of shear connector layout on the behavior of steel-concrete composite beams with interface slip," *Applied Sciences*, vol. 9, no. 1, p. 207, 2019.

[2] Z. Fang, H. Fang, J. Huang, H. Jiang, and G. Chen, "Static behavior of grouped stud shear connectors in steel–precast UHPC composite structures containing thin full-depth slabs," *Engineering Structures*, vol. 252, p. 113484, 2022.

[3] A. El-Zohairy, H. Salim, and H. Shaaban, "Experimental investigation on fatigue behavior of composite beams with different studs arrangements," in *Structures*, 2022, vol. 35: Elsevier, pp. 146-159.

[4] F. Leonhardt, W. Andrä, H. P. Andrä, and W. Harre, "Neues, vorteilhaftes Verbundmittel für Stahlverbund-Tragwerke mit hoher Dauerfestigkeit," *Beton-und Stahlbetonbau,* vol. 82, no. 12, pp. 325-331, 1987.

[5] Y. Xu, X. Liu, B. Wang, and X. Yi, "Residual mechanical properties of composite beams with PBL connectors under fatigue loads," in *Structures*, 2023, vol. 51: Elsevier, pp. 185-195.

[6] J. He *et al.*, "The development of composite bridges with corrugated steel webs in China," in *Proceedings of the Institution of Civil Engineers-Bridge Engineering*, 2021, vol. 174, no. 1: Thomas Telford Ltd, pp. 28-44.

[7] W. Changyu, Y. Shiping, W. Boxue, D. Jianhua, R. Xiaoping, and Z. Xiaoliang, "Research on the transverse flexural performance of T-PBL joints between corrugated steel webs and concrete slabs," in *Structures*, 2022, vol. 44: Elsevier, pp. 1057-1069.

[8] G. Németh, B. Jáger, B. Kövesdi, and N. Kovács, "Experimental investigation of steel-concrete composite push-out tests with embedded corrugated web," *Advances in Structural Engineering*, vol. 25, no. 11, pp. 2332-2347, 2022.

[9] J. Machacek and M. Cudejko, "Composite steel and concrete bridge trusses," *Engineering Structures*, vol. 33, no. 12, pp. 3136-3142, 2011.

[10] H.-Y. Kim and Y.-J. Jeong, "Experimental investigation on behaviour of steel–concrete composite bridge decks with perfobond ribs," *Journal of Constructional Steel Research*, vol. 62, no. 5, pp. 463-471, 2006.

[11] R. Xiao, C. Song, B. Sun, R. Guo, and H. Chen, "Design and experimental study of a replaceable steel-UHPC composite bridge deck," in *Structures*, 2022, vol. 40: Elsevier, pp. 1107-1120.

[12] Y. Shan, Y. Chen, Z. Zong, L. Liu, J. Li, and Z. Li, "Flexural behavior of different types of steel-concrete composite decks with perfobond rib or head stud shear connectors," *Advances in Structural Engineering*, vol. 26, no. 7, pp. 1187-1208, 2023.

[13] C. Liang, Y. Liu, and Y. Liu, "An orthogonal component method for steel girder-concrete abutment connections in integral abutment bridges," *Journal of Constructional Steel Research*, vol. 180, p. 106604, 2021.

[14] S. Liu, X. Ding, X. Li, Y. Liu, and S. Zhao, "Behavior of rectangular-sectional steel tubular columns filled with high-strength steel fiber reinforced concrete under axial compression," *Materials*, vol. 12, no. 17, p. 2716, 2019.

[15] B. Shangguan, Q. Su, J. R. Casas, H. Su, S. Wang, and R. Zhao, "Modeling and Testing of a Composite Steel–Concrete Joint for Hybrid Girder Bridges," *Materials*, vol. 16, no. 8, p. 3265, 2023.

[16] J. Leng, J. Yang, Z. Zhang, Y. Zou, J. Chen, and J. Zhou, "Experimental and numerical investigations on force transfer mechanism of steel-concrete joint in hybrid girder bridges," in *Structures*, 2023, vol. 54: Elsevier, pp. 153-170.

[17] M. H. Nguyen, A. Nakajima, S. Fujiwara, R. Obata, S. Fujikura, and Y. Hirano, "Bending Test of Joint Structure of Precast PC Slab Using Perfobond Strip and its Corresponding Element Test," *Journal of Japan Society of Civil Engineers, Ser. A1 (Structural Engineering & Earthquake Engineering (SE/EE))*, vol. 76, no. 5, pp. II_17-II_28, 2020.

[18] N. M. Hai, S. Fujikura, A. Nakajima, and H. N. Phan, "Experimental investigation on flexural behavior of a precast slab joint with perfobond strips and steel fiber-reinforced mortars," in *Structures*, 2022, vol. 39: Elsevier, pp. 278-292.

[19] K. Aoki, K. Uehira, Y. Tanaka, and K. Takagi, "Development of new joint method for precast railing," in *Proc 9th Symp Res Appl Hybrid Comp Struct*, 2011, pp. 1-8.

[20] Y. Sato and Y. Nishimura, "Shear failure behavior of perfobond rib under shear force at single fracture surface," *Proc Jap Concrete Inst*, vol. 31, pp. 1171-1176, 2009.

[21] N. M. Hai, A. Nakajima, S. Fujikura, T. Murayama, and M. Mori, "Shear behavior of a perfobond strip with steel fiber-reinforced mortar in a condition without surrounding reinforcements," *Materials and Structures*, vol. 53, pp. 1-15, 2020.

[22] E. Oguejiofor and M. Hosain, "Numerical analysis of push-out specimens with perfobond rib connectors," *Computers & structures*, vol. 62, no. 4, pp. 617-624, 1997.

[23] J.-H. Ahn, C.-G. Lee, J.-H. Won, and S.-H. Kim, "Shear resistance of the perfobond-rib shear connector depending on concrete strength and rib arrangement," *Journal of Constructional Steel Research*, vol. 66, no. 10, pp. 1295-1307, 2010.

[24] S. He, Z. Fang, and A. S. Mosallam, "Push-out tests for perfobond strip connectors with UHPC grout in the joints of steel-concrete hybrid bridge girders," *Engineering Structures*, vol. 135, pp. 177-190, 2017.

[25] X. Tan, Z. Fang, and X. Xiong, "Experimental study on group effect of perfobond strip connectors encased in UHPC," *Engineering Structures*, vol. 250, p. 113424, 2022.

[26] G. Ji, E. Zhu, B. Wang, C. Zhu, and S. Li, "Bearing capacity analysis of perfobond rib shear connectors in steel-concrete composite structures," in *Structures*, 2023, vol. 57: Elsevier, p. 105292.

[27] Z. Wang, Q. Li, and C. Zhao, "Ultimate shear resistance of perfobond rib shear connectors based on a modified push-out test," *Advances in Structural Engineering*, vol. 16, no. 4, pp. 667-680, 2013.

[28] S.-H. Kim, J.-H. Ahn, K.-T. Choi, and C.-Y. Jung, "Experimental evaluation of the shear resistance of corrugated perfobond rib shear connections," *Advances in Structural Engineering*, vol. 14, no. 2, pp. 249-263, 2011.

[29] A. Nakajima, S. Koseki, M. Hashimoto, Y. Suzuki, and M. H. Nguyen, "Evaluation of shear resistance of perfobond strip based on simple push-out test," *Journal of Japan Society of Civil Engineers, Ser. A1 (Structural Engineering & Earthquake Engineering (SE/EE))*, vol. 68, no. 2, pp. 495-508, 2012.

[30] Z. Chen, "Experimental study of shear capacity of perfobond connector," *Engineering Meachnics*, vol. 29, no. 12, pp. 349-354, 2012.

[31] *Standard specifications for hybrid structures*, JSCE, 2015.

[32] S. He, Z. Fang, Y. Fang, M. Liu, L. Liu, and A. S. Mosallam, "Experimental study on perfobond strip connector in steel–concrete joints of hybrid bridges," *Journal of Constructional Steel Research*, vol. 118, pp. 169-179, 2016.

[33] S. Zheng, Y. Liu, T. Yoda, and W. Lin, "Parametric study on shear capacity of circular-hole and long-hole perfobond shear connector," *Journal of Constructional Steel Research*, vol. 117, pp. 64-80, 2016.

[34] A. Nakajima, M. Hashimoto, M. Nguyen, and Y. Suzuki, "Shear resisting mechanism and shear resistance evaluation of perfobond strip without penetrating rebar," *Journal of Japan Society of Civil Engineers, Ser. A1 (Structural Engineering)*, 2014.

[35] A. NAKAJIMA and M. H. NGUYEN, "Strain behavior of penetrating rebar in perfobond strip and its evaluation of shear resistance," *Journal of JSCE*, vol. 4, no. 1, pp. 1-18, 2016.

[36] M. H. Nguyen, Y. Hirano, A. Nakajima, S. Fujikura, and R. Niimura, "Experimental evaluation of the shear capacity of perfobond strips with steel fiber-reinforced mortar in narrow joint structures," in *Structures*, 2020, vol. 28: Elsevier, pp. 1173-1186.

[37] H.-T. Thai, "Machine learning for structural engineering: A state-of-the-art review," in *Structures*, 2022, vol. 38: Elsevier, pp. 448-491.

[38] H. Allahyari, I. M. Nikbin, S. Rahimi, and A. Heidarpour, "A new approach to determine strength of Perfobond rib shear connector in steel-concrete composite structures by employing neural network," *Engineering Structures*, vol. 157, pp. 235-249, 2018.

[39] G. Sun, J. Shi, and Y. Deng, "Predicting the capacity of perfobond rib shear connector using an ANN model and GSA method," *Frontiers of Structural and Civil Engineering*, vol. 16, no. 10, pp. 1233-1248, 2022.

[40] M. Nguyen, A. Nakajima, N. Takahashi, M. Mizutori, M. Ono, and S. Fujikura, "Revaluation of shear resistance of perfobond strip considering difference of rib plate and concrete block arrangement," ed: J Jap Soc Civil Eng Ser. A1 (Struct Eng Earthquake Eng (SE/EE)), 2018, pp. 22-27.

[41] K. Nishiumi and M. Okimoto, "Shear strength of perfobond rib shear connector under the confinement," *Doboku Gakkai Ronbunshu*, vol. 1999, no. 633, pp. 193-203, 1999.

[42] U. Yoshitaka, H. Tetsuya, and M. Kaoru, "An experimental study on shear characteristics of perfobond strip and its rational strength equations," in *International symposium on*

connections between steel and concrete, 2001: RILEM Publications SARL, pp. 1066-1075.
[43] T. Hosaka, K. Mitsuki, H. Hiragi, Y. Ushijima, Y. Tachibana, and H. Watanabe, "An experimental study on shear characteristics of perfobond strip and its rational strength equations," *J. Struct. Eng. JSCE*, vol. 46A, pp. 1593–1604, 2000.
[44] H. Furuuchi, T. Ueda, O. Suzuki, and H. Taguchi, "A study on shear transfer capacity of perfobond strip," in *Proceedings of the 6th Symposium on Research and Application of Hybrid and Composite Structure*, 2005, no. 26, pp. 1-8.
[45] K. Fujii, H. Iwasaki, K. Fukada, T. Toyota, and N. Fujimura, "Crack restraint factors in ultimate slip behavior of perfobond strip," *Journal of Japan Society of Civil Engineers, Ser. A*, vol. 64, no. 2, pp. 502-512, 2008.
[46] K. Fujii, Y. Dokan, H. Iwasaki, M. Himukai, K. Mori, and S. Yamaguchi, "Ultimate shear strength of perfobond strip," *J. Jpn. Soc. Civ. Eng. Ser A*, vol. 1, p. 2014, 2014.
[47] Q.-T. Su, W. Wang, H.-W. Luan, and G.-T. Yang, "Experimental research on bearing mechanism of perfobond rib shear connectors," *Journal of Constructional Steel Research*, vol. 95, pp. 22-31, 2014.
[48] S. Guo, S. Hino, K. Yamaguchi, J. Choi, and T. Sonoda, "Bending behavior of steel-concrete composite girder with perfobond shear connector using super-light weight concrete with steel fiber reinforcement," 2008.
[49] R. Yamaguchi, "The push-out test of perfobond strip using high performance concrete," presented at the 8th Symp. Res. Appl. Hybrid Comp. Struct., 2009, 54.
[50] T. Yamada *et al.*, "Experimental study on the mechanical behavior of perfobond rib shear connectors in the rigid connection of a steel-concrete composite portal rigid frame bridge," presented at the 10th Symp. Res. Appl. Hybrid Comp. Struct. , 2013, 59.
[51] I. Norimatsu, T. Tanaka, J. Sakai, and A. Kawano, "Experimental study on mechanical behavior of various kind of shear connectors under constant axial force," presented at the 10th Symp. Res. Appl. Hybrid Comp. Struct., 2013, 20.
[52] T. Ebina, Y. Kutsuna, H. Tategami, and K. Sonoda, "Experimental study on the pull-out resistance of the perfobond rib with flask-shaped steel plate," presented at the Jap. Concr. Ins., 2004.
[53] Y. Taira, K. Furuichi, M. Yamamura, and T. Tominaga, "Experimental Study on Characteristics of Shear Connector using Perforated Plate," presented at the Jap. Concr. Ins., 1998.
[54] C. Ding and H. Peng, "Minimum redundancy feature selection from microarray gene expression data," *Journal of bioinformatics and computational biology*, vol. 3, no. 02, pp. 185-205, 2005.
[55] P. Liashchynskyi and P. Liashchynskyi, "Grid search, random search, genetic algorithm: a big comparison for NAS," *arXiv preprint arXiv:1912.06059*, 2019.
[56] J. Snoek, H. Larochelle, and R. P. Adams, "Practical bayesian optimization of machine learning algorithms," *Advances in neural information processing systems*, vol. 25, 2012.
[57] X. Glorot and Y. Bengio, "Understanding the difficulty of training deep feedforward neural networks," in *Proceedings of the thirteenth international conference on artificial intelligence and statistics*, 2010: JMLR Workshop and Conference Proceedings, pp. 249-256.
[58] K. He, X. Zhang, S. Ren, and J. Sun, "Delving deep into rectifiers: Surpassing human-level performance on imagenet classification," in *Proceedings of the IEEE international conference on computer vision*, 2015, pp. 1026-1034.
[59] T. Fushiki, "Estimation of prediction error by using K-fold cross-validation," *Statistics and Computing*, vol. 21, pp. 137-146, 2011.